

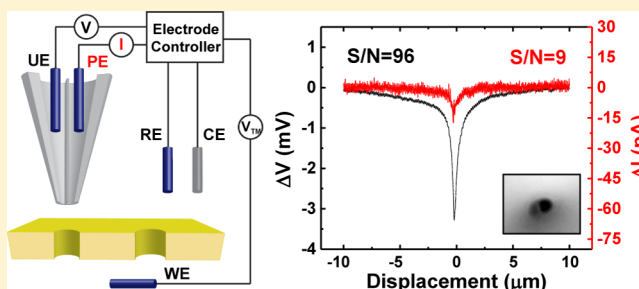
Potentiometric-Scanning Ion Conductance Microscopy

Yi Zhou, Chiao-Chen Chen, Anna E. Weber, Lushan Zhou, and Lane A. Baker*

Department of Chemistry, Indiana University, 800 E. Kirkwood Avenue, Bloomington, Indiana 47405, United States

S Supporting Information

ABSTRACT: We detail the operation mechanism and instrumental limitations for potentiometric-scanning ion conductance microscopy (P-SICM). P-SICM makes use of a dual-barrel probe, where probe position is controlled by the current measured in one barrel and the potential is measured in a second barrel. Here we determine the interaction of these two barrels and resultant effects in quantitation of signals. Effects due to the size difference in pipet tip opening are examined and compared to model calculations. These results provide a basis for quantitation and image interpretation for P-SICM.



■ INTRODUCTION

Scanning ion conductance microscopy (SICM) is a scanning probe microscopy (SPM) technique widely applied for imaging nonconductive substrates, especially biological samples.^{1–3} Although SICM has a number of advantages over other SPM techniques, such as robust control of probe position and noncontact imaging, SICM can be limited by a low signal-to-noise ratio for ion conductance measurements, a condition exacerbated as probe size decreases.⁶ A recently reported modification of SICM, termed potentiometric-scanning ion conductance microscopy (P-SICM), provides a method to overcome some of these limitations.^{7,8} Potentiometric-scanning ion conductance microscopy makes use of a dual-barrel pipet and a five-electrode configuration to realize simultaneous measurement of ion conductance and potential response at the tip of the pipet.

Here, we characterize P-SICM in depth, with an effort to develop quantitative aspects of measurement. Previously, P-SICM has been utilized for differentiation of transcellular and paracellular conductance pathways in epithelial cells with high spatial resolution, which was made possible by the enhanced signal-to-noise ratio of potentiometric measurements.⁷ Additionally, similar to a conventional SICM system, P-SICM can make use of smaller probes for high-resolution imaging, as decreased probe size and decreased probe–sample distance increase potentiometric sensitivity. Until now, mechanisms that enable the sensitivity of P-SICM have not been explored in detail. In this report, a circuit model was proposed and experiments were performed to investigate critical parameters involved in measurement with P-SICM. Experimental results were also compared to simulated results obtained from a potential model proposed by Newman.⁹ Enhancements in potentiometric signal-to-noise ratio were examined and characterized via measurement of single pores in a silicon nitride membrane as probe size and probe–sample distance were varied. These results demonstrate the utility of P-SICM

and serve as a foundation for future studies of synthetic nanopores and biological membranes.

■ EXPERIMENTAL SECTION

Chemicals and Materials. Deionized water (resistivity = 18 MΩ·cm) obtained from a Milli-Q water purification system (Millipore Corp., Danvers, MA) was utilized for solution preparation. Solutions of 0.1 M potassium chloride (Mallinckrodt, Phillipsburg, NJ), filtered with 0.22 μm PVDF filter membranes (Millipore Corp., Danvers, MA), were utilized as electrolyte for P-SICM measurements. To fabricate nanopores with different sizes, TEM grids (TED PELLA INC., Redding, CA) with 250 μm × 250 μm silicon nitride windows of 200 nm thickness, supported by 200 μm thick silicon wafer, were used for focused ion beam (FIB, Zeiss Auriga, Oberkochen, Germany) milling.

Membrane and Probe Fabrication. Circular pores in silicon nitride membranes were milled by FIB. Scanning electron microscopy (SEM) images were used to determine pore diameters (68, 94, and 143 nm). After the FIB milling process, silicon nitride membranes with nanopores were cleaned with piranha solution (3 mL of sulfuric acid and 1 mL of 30% hydrogen peroxide (*caution! piranha reacts violently and is potentially very hazardous*)) at 100 °C for 30 min and subsequently washed three times with degassed, deionized water. After air-drying, membranes were mounted between two chambers of a perfusion cell and sealed with epoxy. Membranes were immersed in 0.1 M KCl solution for measurement. To confirm proper wetting of nanopores, current/voltage curves were measured prior to use in P-SICM experiments.

Nanopipets were initially pulled from quartz theta capillaries (1.2 mm o.d., 0.90 mm i.d.) with a P-2000 laser puller (Sutter, Novato, CA), to obtain pipets with outer diameters of ca. 60 nm for one barrel. FIB was used to mill some tips to larger outer diameters, ca. 175 nm for one barrel. For all measurements here, probes were filled with 0.1 M KCl electrolyte solution,

Received: March 10, 2014

Revised: April 24, 2014

Published: April 28, 2014

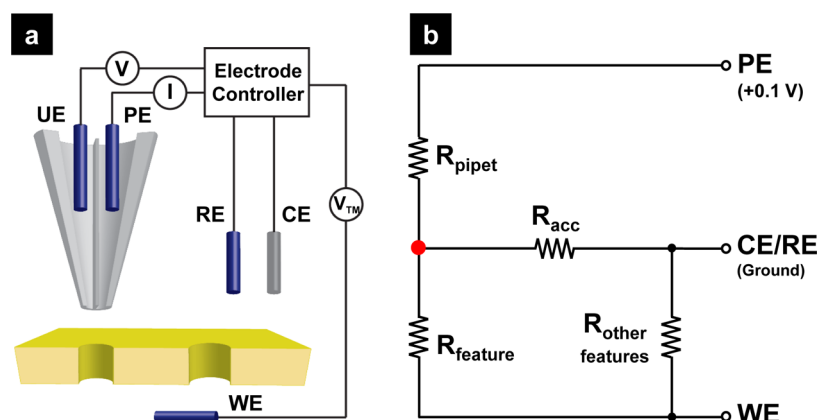


Figure 1. (a) Schematic of the potentiometric-scanning ion conductance microscope (P-SICM). A theta pipet is used to measure local potential difference over nanopores. The barrel with pipet electrode (PE) serves as a current probe to control the probe–sample distance in SICM. The second barrel serves as a potential probe (UE) to measure potential at the pipet tip with respect to the reference electrode (RE). Potential changes are induced by applying a transmembrane potential at the working electrode (WE), reference electrode, and counter electrode (CE). (b) Equivalent circuit of the P-SICM measurement with a nanopore membrane. $R_{\text{other features}}$ indicates the resistance of the pores in parallel with the nanopore investigated with nanopipet.

SICM Instrumentation for Potential Measurement. A modified ScanIC scanning ion conductance microscope with ac feedback mode⁴ (ionscope, London, U.K.) was utilized. As depicted in Figure 1a, a membrane with nanopores was mounted between two chambers of a perfusion cell bathed in an aqueous solution of 0.1 M KCl. In this five-electrode system designed for potential measurement, the pipet electrode (PE) was inserted in one barrel of the theta pipet and was biased at 100 mV with respect to the reference electrode (RE), held in the bath electrolyte of the upper chamber of the perfusion cell. An ion current was generated in this barrel, which is sensitive to the probe–sample distance, and was utilized as a feedback signal to maintain a constant distance above the sample during scanning. A second electrode placed in the other barrel of theta pipet, described here as the potential electrode (UE), served to measure local potential differences with respect to the RE. Potential variations in the vicinity of nanopores were induced by application of transmembrane potentials (V_{TM}) at the working electrode (WE) placed in the lower chamber with respect to RE, where the WE was controlled by a custom electrode driver (electrode control box shown in Figure 1). A Pt counter electrode (CE), also connected to the electrode driver, was utilized to drive the majority of transmembrane current generated by the potential difference between WE and RE to minimize potential fluctuations of RE, and thus to ensure accurate control of potentials of the system. Typical times required to collect an image ($250 \mu\text{m}^2$) are on the order of ~ 10 min. Approach curves were collected in approximately 10 s.

RESULTS AND DISCUSSION

P-SICM Setup and Equivalent Circuit Model. We have described previously a modified five-electrode setup of SICM and the approach to perform potentiometric measurements on epithelial cells, in which apparent conductance of trans- and paracellular pathways were differentiated by localized potential measurements.⁷ Higher signal-to-noise ratio was achieved in potential signal with a potential probe (UE) than the current signal measured simultaneously at PE, which allowed measurement of biological samples with limited conditions amenable to cell cultures (e.g., low applied transmembrane potentials). Compared with a four-electrode setup described previously,⁶ the five-electrode setup shares a similar equivalent circuit model (Figure 1b, the red dot represents where the potential was measured), which was proposed to understand the signals obtained. The same circuit model can be used because, in the five electrode setup of P-SICM, the potential probe measures

the potential difference above a feature of interest with respect to the reference electrode (RE, in the bulk solution). The two electrodes are connected by a differential amplifier with very high resistance ($\sim 10^{13} \Omega$), such that minimal current through the potential probe is negligible and does not disturb the four-electrode circuit. Based on the circuit model, when the nanopipet is positioned over a feature of interest—in this case a nanopore—relationships between the applied voltage, current, and resistance in the system can be solved with consideration of Ohm's law.

$$I_{\text{pipet}}R_{\text{pipet}} + I_{\text{acc}}R_{\text{acc}} = V_{\text{PE}} \quad (1)$$

$$I_{\text{feature}}R_{\text{feature}} + I_{\text{acc}}R_{\text{acc}} = V_{\text{TM}} \quad (2)$$

$$I_{\text{pipet}} + I_{\text{feature}} = I_{\text{acc}} \quad (3)$$

In eq 1, the sum of drops in potential due to the pipet resistance (R_{pipet} , a constant value, determined by the pipet geometry) and access resistance (R_{acc} , a distance-dependent value, determined by the distance between pipet and sample surface) equal the potential applied to the pipet electrode (V_{PE} , +0.1 V). In the other half of the circuit (eq 2), total drops in potential due to the resistance of a feature (R_{feature} , determined by the geometry of the feature within the sensing range of the pipet) and R_{acc} are equal to the applied transmembrane potential (V_{TM}). The sum of the current through the pipet (I_{pipet}) and feature (I_{feature}) is equal to the current through the access resistance (I_{acc}). Thus, application of a transmembrane potential results in a change in the potential drop across the access resistance and a change in the current response of the pipet. The magnitude of change in the pipet current is dependent on the resistance of the nanopore. In the P-SICM setup, the potential probe (UE) reports the potential at the pipet tip, which is assumed to be the potential drop across the access resistance. To improve our efforts at quantitating P-SICM, to better understand intrinsic reasons for the higher signal-to-noise ratio in potential signal, and to validate the circuit model utilized, we have systematically varied the parameters (e.g., membrane pore size, probe–sample distance, pipet tip diameter) in both the model and experiment, and compared the results.

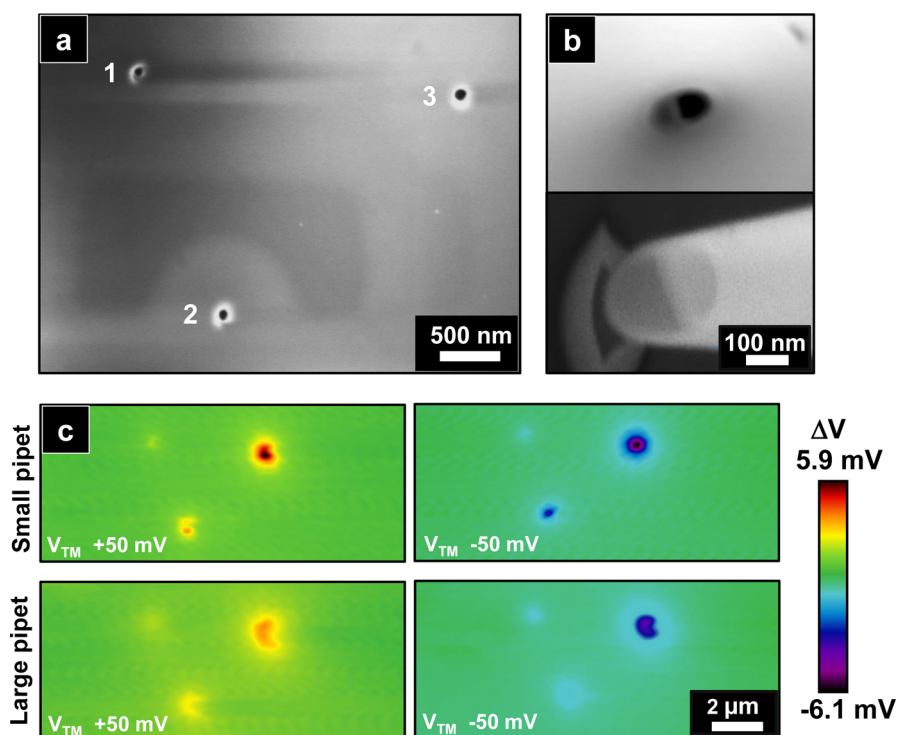


Figure 2. (a) Scanning electron microscopy (SEM) image of silicon nitride nanopore membrane (pore 1, 2, and 3, diameter 68, 94, and 143 nm, respectively). (b) SEM images of small (diameter, ~ 60 nm, for one barrel) and large (diameter, ~ 175 nm, for one barrel) pipets. The SEM for the small pipet is the sibling pipet of small pipet used in the study, fabricated from the same capillary. The large pipet is the same one used in the study and was fabricated by cutting the tip of a small pipet with FIB milling. (c) Potential images obtained with P-SICM for small and large pipets.

A silicon nitride membrane with three different sized pores (Figure 2a, pore 1, 2, and 3; 68, 94, and 143 nm, respectively) was prepared with FIB milling. This membrane was examined by P-SICM with pipets of different tip dimensions (Figure 2b, small pipet and large pipets: 60 and 175 nm in diameter for one barrel). With P-SICM operated in scanning mode (ac feedback), potential images were obtained at both +50 and -50 mV applied transmembrane potential (Figure 2c). In comparison of the images collected, the potential signal measured increases for membrane pores that are larger in size (smaller in resistance) with both small and large pipets. When the sizes of the pipet tip dimensions are compared, the magnitude of potential measured with the small pipet (o.d. ~ 60 nm for each barrel) is higher than for the large pipet (o.d. ~ 175 nm for each barrel). The difference observed is due to a larger probe–sample distance (D_{ps}) utilized when scanning with the large pipet ($D_{ps} = 180$ nm). For the small pipet, feedback parameters allow a smaller probe–sample separation ($D_{ps} = 80$ nm) to be employed.^{10–13} Also, from the potential images, pore geometry is more resolved with the small pipet, while the large pipet results in a semicircle or crescent-shaped image, an artifact which results from the imaging conditions and scan direction (detailed discussion in the Supporting Information). From potential images (Figure 2c), even though the three nanopores imaged are on the order of 100 nm in outer diameter (68, 94, and 143 nm, respectively), the potential distribution around the pore extends to areas on the order of 1 μ m in diameter (at $V_{TM} = 50$ mV, with small pipet, full width at half-maximum values are 433, 500, and 649 nm; with large pipet, full width at half-maximum values are 672, 882, and 1150 nm). This difference in actual pore size and apparent pore size reported from the potentiometric image arises from the size of

the pipet and the extension of the electric field beyond the nanopore perimeter. From these images collected in scanning mode, the utility of P-SICM for measurement of heterogeneous potentials at a surface, in this case for a nanoporous membrane, is evident.

Potential versus Current. To determine the relationship between ion current measured by pipet electrode (PE) and the potential response measured at the potential electrode (UE), line scans over a membrane pore in which the current and potential were simultaneously measured were recorded (Figure 3, over pore 2, 94 nm in diameter, with $V_{TM} = -50$ mV). The ratio of potential change and current change when the pipet was scanned over a pore and over the membrane was found to be equivalent to the pipet resistance. An increase in current was observed when a negative transmembrane potential was applied, the details of which were discussed in previous work.⁶ The potential difference measured when the pipet was over the pore (average of 200 data points obtained within ± 100 nm of the maximum potential) as opposed to over the membrane (average of 400 data points obtained away from pore center) was -2.6 mV (Figure 3a), and current change calculated in the same way was 11.2 pA. This relationship, $\Delta V/(-\Delta I) = 234$ M Ω , agrees well with the small pipet resistance 208 M Ω (measured experimentally). For a larger pipet (Figure 3b), $\Delta V/(-\Delta I) = 2.1$ mV/(37.9 pA) = 56 M Ω , which is also close to direct measurements of pipet resistance (60 M Ω). From the above results, the measured potential change on UE is equal to the potential change of the pipet resistance, which supports assertion that the potential probe is measuring the potential at the pipet tip (same level measured for both barrels of the pipet, Figure 1b, red dot). From the configuration here, the potential difference at the tip is essentially the potential

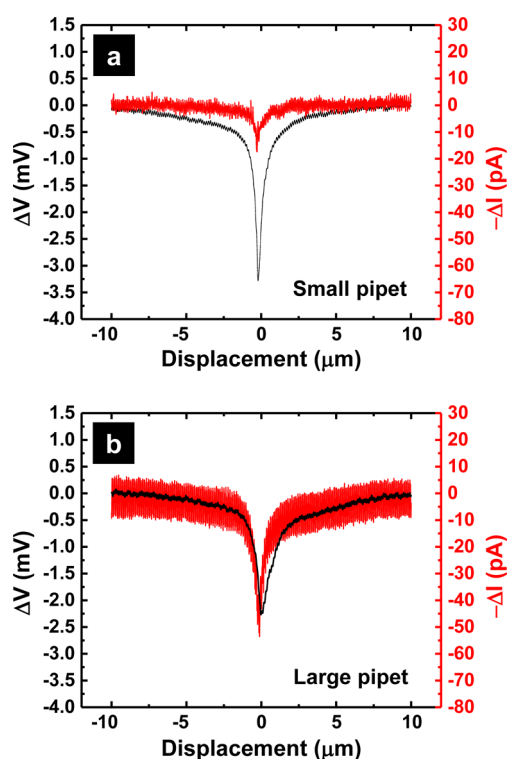


Figure 3. Simultaneously recorded current (red) and potential difference (black) in the small and large theta pipets. The probe was translated over pore 2 (diameter, 94 nm) with a transmembrane potential of -50 mV applied.

drop of the access resistance, relative to the grounded reference electrode. From the circuit model the relationship between current and potential measured at any two different probe positions can be obtained (where I_{pipet} , V_{acc} are from probe position 1 and I'_{pipet} , V'_{acc} from probe position 2), which agrees with experimental results (eq 6).

$$I_{\text{pipet}}R_{\text{pipet}} + V_{\text{acc}} = V_{\text{PE}} \quad (4)$$

$$I'_{\text{pipet}}R_{\text{pipet}} + V'_{\text{acc}} = V_{\text{PE}} \quad (5)$$

$$(5) - (4) \quad \Delta V_{\text{acc}} = -\Delta I_{\text{pipet}}R_{\text{pipet}} \quad (6)$$

The signal-to-noise ratio (S/N = average of signal (within ± 100 nm of maximum value) with background subtracted/standard deviation of noise) can be found for the small pipet (outer diameter ~ 60 nm for each barrel) both when operating as a current probe ($S/N = 8.7$) and as a potential probe ($S/N = 95.6$). Likewise, the case of the large pipet (outer diameter ~ 175 nm for each barrel) as a current probe ($S/N = 7.8$) or a potential probe ($S/N = 73.4$) can be evaluated. From current-displacement traces in Figure 3a and 3b, a difference in the RMS noise, which we believe is related to the capacitance of the differently sized pipets, is observed. Measurement in a potentiometric manner provides significant improvement in the signal-to-noise ratio, which makes measurements of potential differences for biological systems (e.g. cell monolayers) possible, where only small transmembrane potentials can be applied. The signal-to-noise ratios of the current probe for small and large pipets are very similar, though in the case of the small pipet, a smaller probe-sample distance (D_{ps}) is utilized (closer to the source of potential change). For current

probes a small D_{ps} is offset by the larger resistance of the small pipet, which decreases magnitude of the pipet current.

Equation 6 explains why potential measurements result in higher signal-to-noise ratios, relative to current measurements. Simply, the potential probe measures the potential difference between the potential level in the vicinity of the pipet tip and the reference electrode, while the current signal is the result of the potential change at pipet tip divided by the factor of pipet resistance (usually ~ 100 M Ω , nanopipet with diameter 100 nm, in 0.1 M KCl). Especially in the case of small pipets, the result is that current measurement is not as sensitive as potential measurement. Additionally, for local measurements such as those reported with scanning techniques here, a smaller probe can provide higher resolution and reports information from a more localized area. Smaller pipets also benefit from small D_{ps} , where differences in electric fields are greater near the surface of pores.

Potential Approach Curves. When a transmembrane potential is applied across a porous membrane, a potential profile is generated above nanopores present in the membrane. The electric field above pores can be measured by locating the probe at two probe-sample distances, close to and far from the nanopore. The electric field measured in this way can be further converted to conductance, as in epithelial cell studies to evaluate the transport through distinct pathways.^{14–16} In the dual barrel probe, the potential applied at the SICM probe (PE) to generate ion current for distance control is not solely a spectator and can also affect the potential measurement. When a constant transmembrane potential is applied, the potential image can provide a map of potential for each pore in a single scan. However, current density at the pore (a consequence of the transmembrane potential) can cause minor variations in the measured pipet current and to small degrees distorts the probe-sample distance (D_{ps}), as the pipet seeks to maintain feedback. Thus, instead of scanning mode, static measurements, recorded as a function of different probe-sample distance above each pore center, were performed. From potential images obtained in scanning mode (Figure 2c), positions of three pores were identified. In potential approach curve measurement, the pipet was first brought close to the surface directly above a nanopore center in the absence of an applied transmembrane potential. A transmembrane potential V_{TM} ($+200$ or -200 mV) was then applied, and the pipet was withdrawn from the surface, with potential information at each D_{ps} recorded, to generate a plot of potential measured as a function of probe-sample distance. Potential “approach curves” for three different sized pores (pore 1, 2, and 3, 68, 94, and 143 nm in diameter, respectively) were plotted for two different pipets (small and large pipets, 60 and 175 nm o.d. for one barrel) (Figure 4). The potential approach curves are not linear and have two regions: one is close to the pore, where potential changes rapidly, and in a second region, farther from the pore, where change in potential is very small. From previous studies, when a potential is applied to a disk-shaped feature, an electric field, hemispherical in shape, is generated above the feature.⁹ Here, the feature under consideration is the pore present in the membrane. According to models for the distribution of potential by Newman in eqs 7 and 8,⁹ z (the normal distance from the pore) and r (the distance from the axis of symmetry) are functions of the rotational elliptic coordinates ξ , η and the radius of the pore a .

$$z = a\xi\eta \quad (7)$$

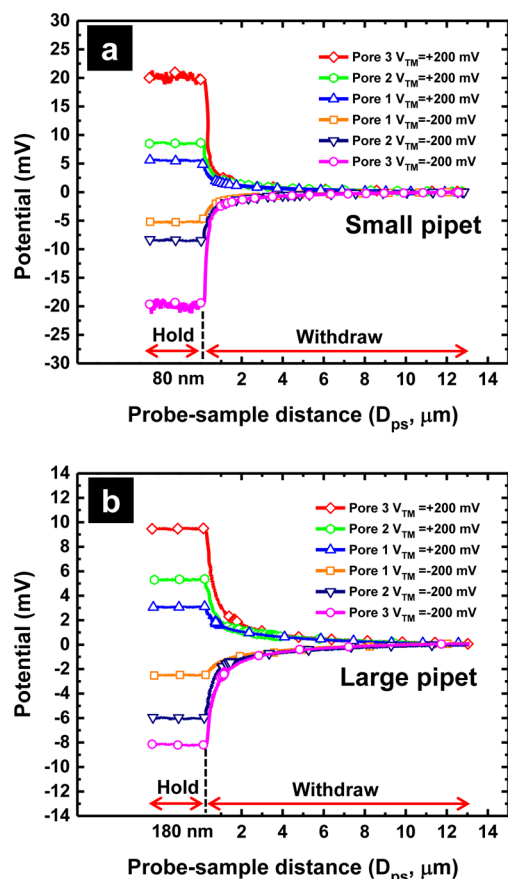


Figure 4. Potential approach curves for small and large pipets (diameter ~ 60 and ~ 175 nm, for one barrel, respectively). Pipets were first brought to the surface with probe-sample distances of 80 and 180 nm, respectively. The transmembrane potential was then turned on (± 200 mV), and the pipet was withdrawn from the surface, to generate a retraction (or in reverse an “approach curve”).

$$r = a\sqrt{(1 + \xi^2)(1 - \eta^2)} \quad (8)$$

The ratio of the potential Φ at a certain position above the pore to the potential at the pore surface Φ_0 can be calculated by eq 9.⁹

$$\Phi/\Phi_0 = 1 - 2/\pi \tan^{-1} \xi \quad (9)$$

The resistance of solution (for one face of the membrane) is given as eq 10 (where κ is the solution conductivity). The electric field decreases from the center of the pore at distances determined by the pore radius. For a uniform cylindrical pore of length l , the resistance is calculated via eq 11.

$$R_{\text{pore opening}} = 1/4\kappa a \quad (10)$$

$$R_{\text{pore}} = l/(\kappa\pi a^2) \quad (11)$$

Finally, the potential at the opening of the pore Φ_0 is given by eq 12.

$$\Phi_0 = V_{\text{TM}} \frac{R_{\text{pore opening}}}{R_{\text{pore}} + 2R_{\text{pore opening}}} \quad (12)$$

Thus, for different pores measured with the same pipet above pore center, a larger pore (larger a) has a higher potential at the same probe-sample distance ($\eta = 1$, $z = a\xi$, same z , smaller ξ), because not only Φ_0 is larger but also the ratio Φ/Φ_0 is larger.

As determined experimentally, the smallest D_{ps} for the two pipets used for the plot are 80 and 180 nm. When measured above the same pore with different pipets, the small pipet with $D_{\text{ps}} = 80$ nm provided a larger potential signal than the large pipet with $D_{\text{ps}} = 180$ nm. Calculated potentials (eqs 9 and 12) at certain distance above nanopore center were plotted (Figure 5) for nanopores with radius 1, 5, 10, 25, and 50 nm, and

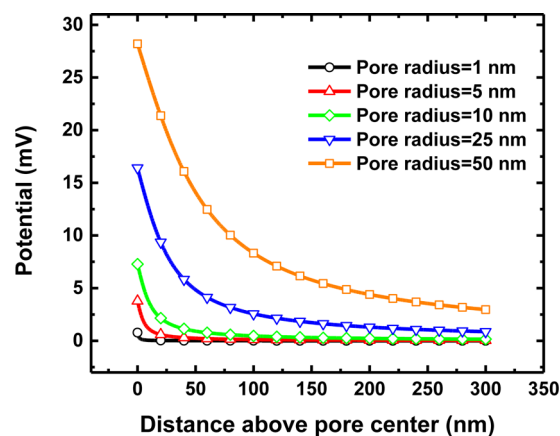


Figure 5. Calculated potentials (potential model) at each distance above the pore center for different sized pores (radius 1, 5, 10, 25, and 50 nm) with 200 mV transmembrane potential applied.

thickness of 200 nm, when 200 mV transmembrane potential is applied. From this plot, influence of the electric field at pores (induced by the transmembrane potential) is limited to distances very near the pore opening. Above certain distances, the difference between these pores is negligible; therefore a smaller probe-sample distance can provide a higher signal and provide better evaluation of transport properties of pores. The probe-sample distance necessary to capture 0.5 mV difference in potential (an easily measured quantity) above each pore is summarized in Table 1. From Table 1, for a pore with radius of

Table 1. Probe-Sample Distance Necessary for a Potential Difference of 0.5 mV

pore radius (nm)	D_{ps} (nm, with $\Delta V = 0.5$ mV)		
	$V_{\text{TM}} = 50$ mV	$V_{\text{TM}} = 200$ mV	$V_{\text{TM}} = 500$ mV
1	N/A	0.6	2.3
5	4.6	23.7	60.0
10	21.7	92.3	231.6
25	129.2	522.2	1305.8
50	446.5	1794.5	4484.2

1 nm, a small transmembrane potential ($V_{\text{TM}} = 50$ mV) results in a potential change above the pore which is too small to measure. When we consider that nominal probe-sample distances are equivalent to the opening of the pipet, at $D_{\text{ps}} = 21.7$ nm ($V_{\text{TM}} = 50$ mV, pore radius = 10 nm) measurement is possible with a smaller pipet (~ 30 nm in diameter). Potential difference above a 5 nm radius nanopore can be measured for higher transmembrane potentials ($V_{\text{TM}} = 200$ or 500 mV). Further reduction of noise levels in the instrument will aid in measurement of small pores.

Effect of Pipet Size and Applied Potential. To determine the relationship between measured potential signals and pore properties, the potential difference (ΔV , with $V_{\text{TM}} = \pm 200$ mV) between two D_{ps} (close $D_{\text{ps}} \sim 100$ nm and far $D_{\text{ps}} \sim$

12.5 μm) are plotted as a function of pore conductance (reciprocal of pore resistance) in Figure 6. In addition to the

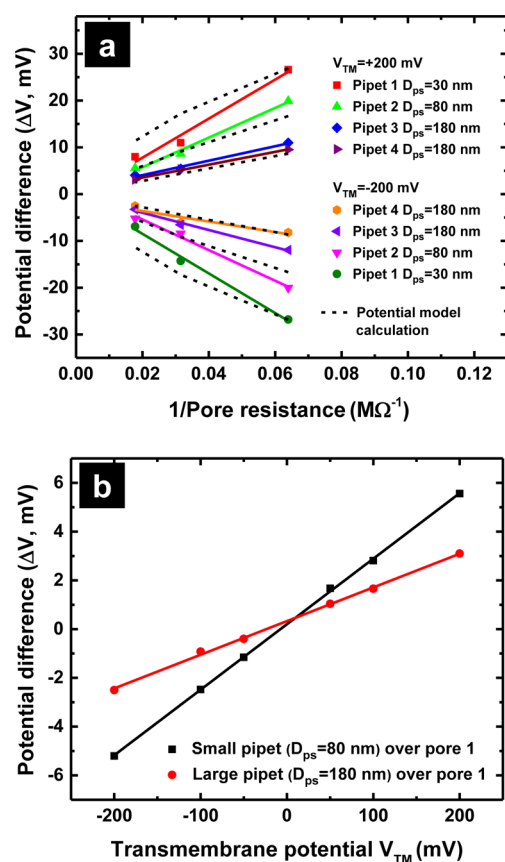


Figure 6. (a) Potential difference measured for four different sized pipets (pipet 1–4, ~40, 60, 175, and 175 nm, in diameter for one barrel) above each pore at two probe–sample distance ($D_{\text{ps}} = 30, 80$, or 180 nm and $D_{\text{ps}} = 12.5 \mu\text{m}$, close and far), plotted with the reciprocal of pore resistance. Dashed lines represent the calculated potential obtained by potential model eqs 7–12. (b) Relationship of potential difference at two D_{ps} with different transmembrane potentials measured by small and large pipets (diameter, ~60 and ~175 nm, for one barrel, respectively) over the pore 1 (68 nm in diameter).

pipet sizes discussed above (pipet 2, the “small” pipet, ~60 nm in diameter for one barrel, and pipet 3, the “large” pipet, ~175 nm in diameter), two additional pipets (pipet 1, ~40 nm and pipet 4, ~175 nm in diameter for one barrel) were utilized to examine the electric field above nanopores. Almost all four pipets displayed a linear relationship between the measured potential difference and the pore conductance (seven lines have R^2 in the range of 0.98–0.99, only one line has a poor R^2 of 0.89), which indicates that the measured potential difference can be used to describe the property of the membrane pore. For pipets of similar size (pipets 3 and 4, ~175 nm in diameter, size confirmed by pipet currents and SEM images) fairly consistent data can be obtained for the same feature. For pipet 1 (~40 nm in diameter), which has the smallest D_{ps} (~30 nm), the largest potential difference ($\Delta V = V_{30 \text{ nm}} - V_{12.5 \mu\text{m}}$, ~26 mV) was obtained and provided the largest difference in signal for the three pore sizes measured here. Linearity between potential measurements and the pore conductance may only be valid in the range of pore sizes studied here (detailed discussion in Supporting Information). In Figure 6a, the calculated potential levels based on eqs 7–12 at each distance (probe–

sample distance) above the pore center ($r = 0$) are also plotted and compared with the measured values. Measured potentials above a pore by P-SICM at fixed D_{ps} agree well with the calculated potential level with the same D_{ps} above the pore. Of note, when the pore size gets smaller, the measured potential is consistently lower than the calculated value, which is primarily due to the large size of pipet relative to the pore, a factor is not considered in the calculation. Simulated values from the circuit model, which included the factor that the pipet disturbed the potential above the nanopore, also match with the measured signal very well (Figure S2, Supporting Information), which indicates that the circuit model also provides a good description of the P-SICM system and allows for quantitative estimates of the pore resistance to be made from the experimental potential difference and the circuit model.

Pipets 2 (diameter = 60 nm, $D_{\text{ps}} = 80$ nm) and 3 (diameter = 175 nm, $D_{\text{ps}} = 180$ nm) were also used to measure potential differences above pore 1 (diameter = 68 nm) under different transmembrane potentials (± 50 , ± 100 , and ± 200 mV, Figure 6b). A linear relationship ($R^2 = 1.00$ for both pipets) was obtained between the applied transmembrane potential and measured potential on UE. The P-SICM signal recorded was proportional to applied potential, which further confirms the circuit model (eq 2) and agrees with eq 12. However, from these two linear relationships, when V_{TM} is 0, a potential difference between two D_{ps} ($\Delta V = V_{30 \text{ nm}} - V_{12.5 \mu\text{m}}$) is observed. This can be caused by several factors, e.g., deviation from different measurements, but is primarily a result of the access resistance, which increases with the decreasing D_{ps} . When D_{ps} is large, with 100 mV applied on PE and no transmembrane potential, the access resistance is negligible, $I_{\text{pipet}} = V_{\text{PE}}/R_{\text{pipet}}$. When the pipet gets closer, $I_{\text{pipet}} = V_{\text{PE}}/(R_{\text{pipet}} + R_{\text{acc}})$, which results in decrease in the pipet current and increase in the potential (eq 6, 0.2 mV for small pipet) measured at the pipet tip. This indicates the potential applied on PE indeed affects the measured potential difference, which can also be predicted in the circuit model calculation. However, according to the circuit model, the measured potential at pipet tip is proportional to applied transmembrane potential and the 100 mV applied on pipet is a constant offset for the same pipet (eq S9, Supporting Information). This means the potential applied to the pipet will affect the amplitude of potential difference measured but will not affect the change of potential difference with different transmembrane potentials (slope in Figure 6b), as the slope is only a function of resistors in the system. As in the previous P-SICM experiment with epithelial cell membranes, a triangular wave transmembrane potential was applied, and the slope of the potential change measured by nanopipet was utilized to calculate localized conductance.⁴ In this way, the offset of potential measured due to the 100 mV bias on pipet was removed by consideration of the slope of potential change. These results demonstrate that P-SICM is a quantitative method, and that potential signals can be used not only to compare the transport properties of features with small differences but also to estimate the resistance of features measured with the proposed circuit model.

CONCLUSION

Through experiments on nanopore samples of well-defined geometries, mechanisms and subtleties of P-SICM have been studied and understood. The proposed circuit model and the relationship between current and potential probes confirm that potential measured is the potential drop on access resistance.

Smaller pipets are shown to provide a much higher signal-to-noise ratio in potential measurement, but not in current measurement. From the circuit model and measured potentials, pore resistance can be estimated, which increases the quantitative nature of P-SICM. The measured pipet potential and applied potential relationship further validate previous P-SICM measurements at cell interfaces and elucidate the importance of multiple transmembrane potentials to remove effects from the potential applied in the current measuring barrel of P-SICM.

■ ASSOCIATED CONTENT

● Supporting Information

Nanopipet pulling parameters, discussion of artifact in potential images, and details of circuit model calculation. This material is available free of charge via the Internet at <http://pubs.acs.org>.

■ AUTHOR INFORMATION

Corresponding Author

*E-mail lanbaker@indiana.edu; Ph (812) 856-1873; Fax (812) 856-8300 (L.A.B.).

Notes

The authors declare no competing financial interest.

■ ACKNOWLEDGMENTS

The National Science Foundation (CHE0847642) is acknowledged for support on this work. We also thank the assistance of Andy Alexander and John Poehlman (Electronic Instrument Services, Indiana University) on instrumentation. A.E.W. acknowledges the Quantitative Chemical Biology program at Indiana University for support. Access to instrumentation in the Nanoscale Characterization Facility at Indiana University is also acknowledged.

■ REFERENCES

- (1) Hansma, P. K.; Drake, B.; Marti, O.; Gould, S. A. C.; Prater, C. B. The Scanning Ion-Conductance Microscope. *Science* **1989**, *243* (4891), 641–643.
- (2) Korchev, Y. E.; Bashford, C. L.; Milovanovic, M.; Vodyanoy, I.; Lab, M. J. Scanning Ion Conductance Microscopy of Living Cells. *Biophys. J.* **1997**, *73* (2), 653–658.
- (3) Shevchuk, A. I.; Gorelik, J.; Harding, S. E.; Lab, M. J.; Klenerman, D.; Korchev, Y. E. Simultaneous Measurement of Ca^{2+} and Cellular Dynamics: Combined Scanning Ion Conductance and Optical Microscopy to Study Contracting Cardiac Myocytes. *Biophys. J.* **2001**, *81* (3), 1759–1764.
- (4) Chen, C.-C.; Zhou, Y.; Baker, L. A. Scanning Ion Conductance Microscopy. *Annu. Rev. Anal. Chem.* **2012**, *5* (1), 207–228.
- (5) Sánchez, D.; Johnson, N.; Li, C.; Novak, P.; Rheinlaender, J.; Zhang, Y.; Anand, U.; Anand, P.; Gorelik, J.; Frolenkov, G. I.; Benham, C.; Lab, M.; Ostanin, V. P.; Schäffer, T. E.; Klenerman, D.; Korchev, Y. E. Noncontact Measurement of the Local Mechanical Properties of Living Cells Using Pressure Applied Via a Pipette. *Biophys. J.* **2008**, *95* (6), 3017–3027.
- (6) Zhou, Y.; Chen, C.-C.; Baker, L. A. Heterogeneity of Multiple-Pore Membranes Investigated with Ion Conductance Microscopy. *Anal. Chem.* **2012**, *84* (6), 3003–3009.
- (7) Chen, C.-C.; Zhou, Y.; Morris, C. A.; Hou, J.; Baker, L. A. Scanning Ion Conductance Microscopy Measurement of Paracellular Channel Conductance in Tight Junctions. *Anal. Chem.* **2013**, *85* (7), 3621–3628.
- (8) Zhou, Y.; Chen, C.-C.; Weber, A. E.; Zhou, L.; Baker, L. A.; Hou, J. Potentiometric-Scanning Ion Conductance Microscopy for Measurement at Tight Junctions. *Tissue Barriers* **2013**, *1* (4), e25585.
- (9) Newman, J. Resistance for Flow of Current to a Disk. *J. Electrochem. Soc.* **1966**, *113* (5), 501–502.
- (10) Ying, L. M.; Bruckbauer, A.; Zhou, D.; Gorelik, J.; Shevchuk, A.; Lab, M.; Korchev, Y.; Klenerman, D. The Scanned Nanopipette: A New Tool for High Resolution Bioimaging and Controlled Deposition of Biomolecules. *Phys. Chem. Chem. Phys.* **2005**, *7*, 2859–2866.
- (11) Edwards, M. A.; Williams, C. G.; Whitworth, A. L.; Unwin, P. R. Scanning Ion Conductance Microscopy: A Model for Experimentally Realistic Conditions and Image Interpretation. *Anal. Chem.* **2009**, *81* (11), 4482–4492.
- (12) Korchev, Y. E.; Milovanovic, M.; Bashford, C. L.; Bennett, D. C.; Sviderskaya, E. V.; Vodyanoy, I.; Lab, M. J. Specialized Scanning Ion-Conductance Microscope for Imaging of Living Cells. *J. Microsc. (Oxford, U. K.)* **1997**, *188*, 17–23.
- (13) Shevchuk, A. I.; Frolenkov, G. I.; Sanchez, D.; James, P. S.; Freedman, N.; Lab, M. J.; Jones, R.; Klenerman, D.; Korchev, Y. E. Imaging Proteins in Membranes of Living Cells by High-Resolution Scanning Ion Conductance Microscopy. *Angew. Chem., Int. Ed.* **2006**, *45* (14), 2212–2216.
- (14) Gitter, A. H.; Bertog, M.; Schulzke, J. D.; Fromm, M. Measurement of Paracellular Epithelial Conductivity by Conductance Scanning. *Pfluegers Arch.* **1997**, *434* (6), 830–840.
- (15) Cereijido, M.; Meza, I.; Martinezpalomo, A. Occluding Junctions in Cultured Epithelial Monolayers. *Am. J. Physiol. Cell Physiol.* **1981**, *240* (3), C96–C102.
- (16) Frömter, E. The Route of Passive Ion Movement through the Epithelium of *Necturus* Gallbladder. *J. Membr. Biol.* **1972**, *8* (1), 259–301.